Characterization of Structure and Metal Ions Specificity of Co^{2+}-Binding RNA Aptamers†

Jan Wrzesinski* and Jerzy Ciesiolka

Institute of Bioorganic Chemistry, Polish Academy of Sciences, Noskowskiego 12/14, 61-704 Poznan, Poland

Received December 10, 2004; Revised Manuscript Received February 26, 2005

ABSTRACT: Studies on RNA motifs capable of binding metal ions have largely focused on Mg^{2+}-specific motifs, therefore information concerning interactions of other metal ions with RNA is still very limited. Application of the in vitro selection approach allowed us to isolate two RNA aptamers that bind Co^{2+} ions. Structural analysis of their secondary structures revealed the presence of two motifs, loop E and "kissing" loop complex, commonly occurring in RNA molecules. The Co^{2+}-induced cleavage method was used for identification of Co^{2+}-binding sites after the determination of the optimal cleavage conditions. In the aptamers, Co^{2+} ions seem to bind to N7 atoms of purines, inducing cleavage of the adjacent phosphodiester bonds, similarly as is the case with yeast $tRNA^{Phe}$. Although the in vitro selection experiment was carried out in the presence of Co^{2+} ions only, the aptamers displayed broader metal ions specificity. This was shown by inhibition of Co^{2+}-induced cleavages in the presence of the following transition metal ions: Zn^{2+}, Cd^{2+}, Ni^{2+}, and $Co(NH_3)_6^{3+}$ complex. On the other hand, alkaline metal ions such as Mg^{2+}, Ca^{2+}, Sr^{2+}, and Ba^{2+} affected Co^{2+}-induced cleavages only slightly. Multiple metal ions specificity of Co^{2+}-binding sites has also been reported for other in vitro selected or natural RNAs. Among many factors that influence metal specificity of the Co^{2+}-binding pocket, chemical properties of metal ions, such as their hardness as well as the structure of the coordination site, seem to be particularly important.

Metal ions play important roles in the cell of all known living organisms, from bacteria to animals. They are indispensable constituents of two cell components, proteins and nucleic acids. In protein enzymes, metal ions are cofactors that influence their proper folding and are needed for enzymes' catalytic activities. Enzymes use a variety of metal ions, which participate directly in their catalytic mechanisms. Among them are not only the most abundant alkaline earth metal ions but also rare metal ions, including Cu (superoxide dismutase), Ni (urease), Zn (carbonic anhydrase), Fe (peroxidase), Mo (nitrogenase), and V (chloroperoxidase) (*1*, *2*). Furthermore, it is well-documented that most proteins create metal ion binding pockets, which are characterized by high metal affinity and specificity. Therefore, enzymes might be classified by metal ions that they specifically bind, that is, cooper enzymes, nickel enzyme, zinc enzymes, and so forth.

Nucleic acids are also good targets for a variety of metal ions. Generally, alkaline metals bind to exposed phosphate groups of the DNA helix, thus, stabilizing its structure. Interactions of the transition metal ions, preferentially with bases, show opposite effects and destabilize the DNA structure (*3*). Folded RNA structures bind metal ions in two different ways: many weak binding sites with affinity within the millimolar range and only a few strong binding sites with affinity within the micromolar range have usually been found (*4*−*7*). Weakly bound metal ions neutralize negative charges of RNA phosphate groups by simple electrostatic interactions; however, in their strong binding sites, metal ions interact additionally with bases. In the latter interactions, mainly N3 and N7 of guanine and adenine, O4 of uracil, and N3 of cytosine atoms are involved via the inner or outer coordination sphere of metals. However, affinities of metal ions to RNA molecules are much lower than those determined for protein enzymes; for instance, Mg^{2+} bound to tRNA shows a K_d of 10−100 μM (*5*), whereas Zn^{2+} bound to carbonic anhydrase shows a $K_d \sim 1$ pM (*8*). Weakly bound metal ions are necessary for folding of an RNA into its correct secondary structure; however, strongly bound ions play a more important role as they are essential in the formation of the RNA tertiary structure (*9*). The discovery of ribozymes, particular RNA molecules with catalytic activity, has rapidly increased the interest in RNA−metal ions interactions (*10*−*11*). Most ribozymes are in vitro efficient in millimolar concentration of divalent metal ions such as Mg^{2+}, Ca^{2+}, and Mn^{2+} (*5*). Participation of metal ions in the folding of ribozymes and their direct involvement in the catalytic mechanisms, similar to protein enzymes, have been proposed (*12*).

The majority of data on metal ion−RNA interactions have been obtained by means of several physical and biochemical methods using physiological concentration of Mg^{2+} ions (*13*). However, in addition to Mg^{2+} and other alkaline metals, transitions metals such as Fe^{2+}, Zn^{2+}, or Co^{2+} are also present in the cell. Information concerning interactions of these transition metals with RNA is very limited, though. Recently, we have focused our interest on Co^{2+}, an exceptional transition metal ion, which actively participates in both

† This work was supported by Grant No. 6 P04A 081 21, from the Polish Committee for Scientific Research.

* To whom correspondence should be addressed. E-mail, wrzesinj@ibch.poznan.pl; phone, +48 61 8528503; fax, +48 61 8520532.

10.1021/bi047397u CCC: $30.25
Published on Web 03/31/2005

protein and RNA catalytic processes. Several protein enzymes that coordinate this ion in their catalytic sites have been described (*14*). However, the hammerhead (*15*) and delta (*16*) as well as *glm S* (*17*) ribozymes undergo efficient self-cleavage in the presence of millimolar concentrations of Co^{2+}. To find RNA motifs with the affinity to Co^{2+}, we applied an in vitro selection approach. This approach has been shown to be well-suited to isolate RNA molecules capable of binding several low molecular ligands, such as amino acids, antibiotics, organic dyes, and some metabolites (reviewed in refs *18* and *19*).

Herein, we describe the structure and properties of two aptamers that specifically bind Co^{2+} ions, which were isolated from a combinatorial RNA library by an in vitro selection procedure. Special attention is paid to the metal ion binding properties of the selected aptamers, and factors influencing metal ions specificity of Co^{2+}-binding sites are discussed.

MATERIALS AND METHODS

Materials. T7 RNA polymerase, polynucleotide kinase, *Taq* polymerase, restriction enzymes, dNTPs, and NTPs were purchased from MBI Fermentas. AMV reverse transcriptase, T1, and S1 nucleases were from Promega. (γ-^{32}P)ATP was from ICN. NTA resin was from Novagen. All chemicals and salts were from Serva or Fluka.

Construction of RNA Library. All oligodeoxynucleotides used in the construction of the DNA templates were deprotected after synthesis and purified on denaturing 8% polyacrylamide gels. DNA bands were excised, eluted with 0.3 M sodium acetate, pH 5.2, and 1 mM EDTA, and precipitated with 3 vol of ethanol; DNA was recovered by centrifugation and dissolved in TE buffer. The DNA template for in vitro transcription of the RNA library was prepared using two DNA oligomers: LM72 (5′-CGAAGCTTG-CATATGCTACGCTGAG GCN_{23}GCCTACAGCCTAACG-TATGCCC-3′) and LM47 (5′-*GCGAGCTCTAATACGACT-CACTAT A*GGGCATACGTTAGGCTGTAGGC-3′) (letters in italics mark T7 RNA polymerase promoter, complementary sequences are underlined, N_{23} indicates random 23 nucleotide-long sequence). Equimolar amounts of both oligomers were annealed, and a double-stranded DNA template was generated by PCR in standard conditions (*20*). The PCR reaction was performed for five cycles of 30s at 94 °C, 30s at 48 °C, and 1 min at 72 °C. The double-stranded DNA template was extracted with phenol/chloroform (1:1), precipitated, dissolved in TE buffer, and used in a transcription reaction.

The in vitro transcription reaction was performed using a T7 RNA polymerase system (*21*). To obtain an RNA oligomer with a hydroxyl group at its 5′-end, 4 mM guanosine was added to the transcription mixture. The RNA combinatorial library was labeled at the 5′-end using (γ-^{32}P)ATP and T4 polynucleotide kinase under standard conditions.

In Vitro Selection. The selection procedure was adopted from previous selections of RNA aptamers that specifically bind Zn^{2+} and Ni^{2+} ions (*22*−*24*). Briefly, 200 μL of the NTA resin (Novagen) was taken into an Eppendorf tube and washed twice with 200 μL of water, and the supernatant was removed by centrifugation. Subsequently, the resin was charged with Co^{2+} by applying 500 μL of a 100 mM $CoCl_2$ solution, and after removing excess of Co^{2+}, the resin was washed once with 500 μL of water and, subsequently, three times with the same volume of buffer A (20 mM Hepes−NaOH, 400 mM NaCl, and 1 mM $MgCl_2$). The 5′-^{32}P-labeled RNA library in buffer A was renatured and mixed with the resin with gentle agitation for 5 min. In the first selection step (preselection), the resin not charged with Co^{2+} was used. Unbound RNA was removed by centrifugation, then the resin was washed seven times with 600 μL of buffer A and finally six times with 200 μL of buffer A with 2 mM $CoCl_2$ with gentle agitation for 5 min. The RNA was precipitated with ethanol and reverse-transcribed with Superscript reverse transcriptase. Subsequently, cDNA was amplified by PCR, purified by phenol−chloroform extraction, and transcribed using T7 RNA polymerase.

The DNA library from the final step of selection was digested with *Hind*III and *Sac*I and ligated into pUC19 vector. *Escherichia coli* JM 109 cells were transformed with the ligation mixture, and plasmids from individual clones were sequenced using standard dideoxy sequencing procedure.

RNA Probing. The Pb^{2+}-induced cleavage reaction was carried out with 5′-end-labeled RNA in the presence of 8 μM concentration of unlabeled RNA in buffer containing 10 mM Tris-HCl, pH 7.2, 40 mM NaCl, and 10 mM $MgCl_2$. Prior to the reaction, the standard denaturation−renaturation procedure was used. The RNA was heated to 65 °C and then slowly cooled to 25 °C. Other reaction conditions are specified in the figure legends. All reactions were stopped by mixing with an equal volume of 8 M urea/dyes with 10 mM EDTA.

For S1 nuclease mapping, identical conditions to those described for the Pb^{2+}-induced cleavage were used, except that 1 mM $ZnCl_2$ was additionally added. To terminate the reactions, a mixture of 8 M urea/dyes with 10 mM EDTA was added and the samples were immediately frozen on dry ice.

Chemical modification of RNA was essentially performed as described earlier (*25*), and 10 mM concentration of $MgCl_2$ in reaction buffers was applied. Dimethyl sulfate (DMS) and 1-cyclohexyl-3-(2-morpholinoethyl)carbodiimide metho-*p*-toluene sulfonate (CMCT) were used. DMS methylates unpaired N1 of adenine and N3 of cytosine, while CMCT reacts with both unpaired guanine and uracil at the N1 and N3 positions, respectively. Sites of modification were determined using the reverse transcriptase primer extension method.

Co^{2+}-Induced RNA Cleavage. Prior to reaction, 5′-end-labeled RNA, supplemented with 8 μM unlabeled RNA was renatured in 50 mM Hepes−NaOH, pH 8.0, and 40 mM NaCl by heating to 65 °C and cooling down slowly to 25 °C. Subsequently, $CoCl_2$ was added, and the reaction proceeded at 37 °C for time intervals specified in the figure legends. The effects of the presence of different metal ions on Co^{2+}-induced cleavage were tested using 1 and 5 mM concentration of the appropriate metal ions and 2 mM concentration of Co^{2+} at 37 °C for 3 h. Cleavage reactions were stopped by mixing with an equal volume of an 8M urea/dyes with 20mM EDTA solution, and samples were loaded on 12% polyacrylamide, 0.75% bisacrylmide, and 7M urea gels. Electrophoresis was performed at 65 W for 3 h,

followed for autoradiography at −70 °C with an intensifying screen. For quantitative analysis, gels were exposed to phosphoimaging screen and quantified using a Typhoon 8600 imager with ImageQuant software (Molecular Dynamics). For k_{obs} determination at appropriate time intervals, the Co^{2+} cleavage reaction aliquots were taken and quantified on gel, and subsequently, the logarithm of the percent uncleaved RNA was plotted as a function of time. The negative slope of the least-squares plot yielded the cleavage rate (*26*).

To assign the cleavage sites, products of the cleavage reactions were run along with the products of alkaline degradation and limited T_1 nuclease digestion of the same RNA molecule. The alkaline hydrolysis ladder was generated by incubation of ^{32}P-end-labeled RNA with 5 vol of formamide/2 mM $MgCl_2$ in boiling water for 15 min. Partial T1 nuclease digestion was performed in denaturing conditions (50 mM sodium citrate, pH 4.5, and 7 M urea), with 0.1 unit of the enzyme. The reaction mixture was incubated for 10 min at 55 °C.

Determination of K_d Values for Binding of Co^{2+} Ions to RNA Aptamers. First, the K_d values were determined using isocratic elution of RNA from the NTA−Co^{2+} column (*27*) and calculated from the equation $K_d = L[(V_{el} - V_n)/(V_e - V_{el})]$, where L is the free ligand concentration used to isocratically elute RNA loaded onto the affinity column, V_{el} is the median elution volume of RNA eluted in the continuous presence of free ligand, V_e is the median elution volume measured in the absence of free ligand in the column buffer, and V_n is the volume at which an RNA population having no interaction with the column would elute. The other method applied for the determination of K_d values in solution employs the dependence of Co^{2+}-promoted cleavage on metal ion concentration. The Co^{2+} concentration at which the extent of the cleavage reaction reached half of the maximum yield was taken as the K_d value.

RESULTS

Selection of Co^{2+}-Binding Aptamers. For in vitro selection of Co^{2+}-binding aptamers from a library of approximately 7×10^{13} different RNA sequences, the NTA resin with immobilized Co^{2+} ions was used. Since Co^{2+} ions usually contain six coordination sites and four sites were occupied upon complexation with the resin, thus, only two sites remained available for interaction with other ligands (Figure 1A). The RNA library consisted of a randomized region of 23 nucleotides, flanked by two fixed RNA stretches for reverse transcription and PCR amplification (Figure 1B). The RNA library was mixed with the resin, then weakly bound molecules were washed out, and subsequently, Co^{2+} binders were eluted with buffer supplemented with 2 mM Co^{2+} ions. After 15 rounds of selection, 14% of loaded RNA was Co^{2+}-eluted and no further enrichment of this fraction was seen in the next round (Figure 1C). Heterogenity of the RNA pools after the 15th and 16th rounds of selection was assayed with T1 ribonuclease (*22*). The patterns of limited digestion of the initially randomized regions were very similar in both RNA pools; therefore, the pool after the 15th round of selection was cloned and sequenced. Among 32 clones, two unique sequences were identified (aptamers no. 18 and no. 20, Figure 1D). The first sequence was repeated six times; however, the second sequence dominated and occurred in

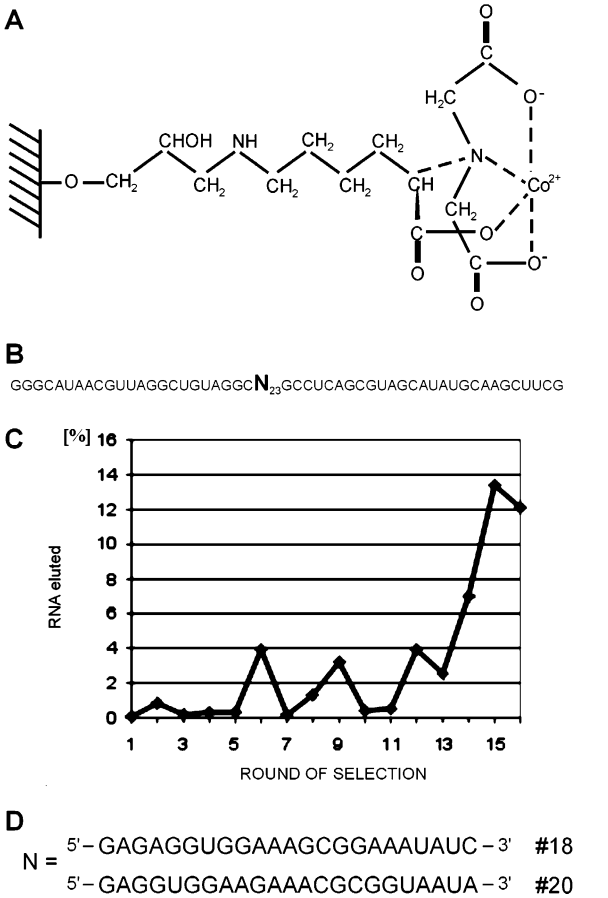

FIGURE 1: In vitro selection of Co^{2+}-binding aptamers: (A) structure of NTA resin with bound Co^{2+} used in selection procedure; (B) construction of the initial RNA library, the sequences of constant regions are shown, N_{23} marks a random region; (C) percentage of RNA pool eluted from the Co^{2+}−NTA resin after each selection cycle, RNA was eluted from resin with the buffer 20 mM Hepes−NaOH, pH 7.0, 400 mM NaCl, 1mM $MgCl_2$, and 2 mM $CoCl_2$; (D) the nucleotide sequences in the initially randomized region of two dominant aptamers no. 18 and no. 20.

24 clones. Additionally, two orphan sequences were found. Both the most abundant Co^{2+} aptamers, namely, no. 18 and no. 20, contained a high amount of purine residues, over 74%. The aptamers were characterized in detail in terms of their K_d constants, Co^{2+}-binding site structure, and metal-binding specificity. The K_d values determined by isocratic elution of RNA from NTA−Co^{2+} resin were 3.16 ± 0.22 and 1.10 ± 0.15 mM, for aptamers no. 18 and no. 20, respectively.

Probing of Aptamers' Secondary Structures. The secondary structures of aptamers no. 18 and no. 20 were analyzed using a Pb^{2+}-induced cleavage method and S1 nuclease digestion as well as chemical modification. It is well-established that Pb^{2+} ions induce breakage of phosphodiester bonds preferentially in single-stranded RNA regions or in regions of high flexibility; thus, these ions are very useful for determination of RNA secondary structures (*28*). The probing experiments were carried out with different concentrations of Pb^{2+} ions (Figures 2 and 3). Clearly, aptamers no. 18 and no. 20 possess similar stem−loop secondary structures; however, they differ in regard to the size of their apical loops. Aptamer no. 18 consists of an 18-nucleotide loop closed with a double-stranded stem. The entire loop undergoes Pb^{2+}-induced cleavage, whereas the G23−C45

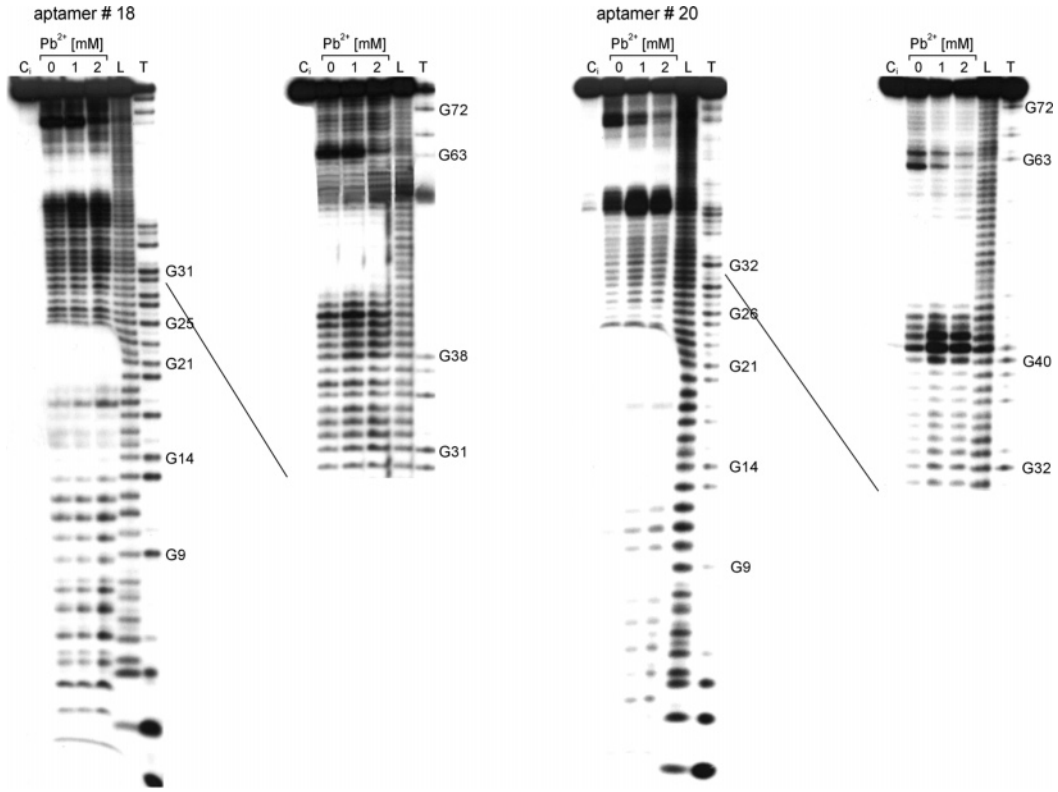

FIGURE 2: Pb^{2+} probing of the structure of selected aptamers no. 18 and no. 20. Reactions were performed with 5′-end-labeled RNA at 25 °C for 10 min. Lanes are labeled as follows: C, reaction control; L, formamide ladder; T, limited hydrolysis by RNase T1. Guanine residues are labeled on the right. For both aptamers, short and long runs of the gel are shown.

and A24−U44 stretches, that are base-paired, are resistant to cleavage. The major cleavages occur at the 3′-side of the loop, at nucleotides A41 and U42. In aptamer no. 20, a larger loop with 22 nucleotides exists. Additionally, the 36-CGCG-39 region within the loop is not cleaved, and the major Pb^{2+} cleavages are shifted toward the 5′-side of the loop of the 40-GUA-42 region. Susceptible to Pb^{2+} cleavage is also the bottom segment of stem region G3−A12/U55−64 (Figure 3), which consists of several A−U base pairs and two mismatches, C8−A59 and G13−G58, as well as a nonstandard base pair, U10−G57. Because of such helix disturbances, this region is probably less thermodynamically stable than the top segment of the stem, which contains at least six G−C base pairs.

The patterns of S1 digestion of both aptamers are more specific (Figure 4A,B). Interestingly, the RNA stretches immediately adjacent to the helical stem are not digested by the enzyme. Additionally, in aptamer no. 20, the A30−G39 region is also resistant to S1 digestion (Figure 4A,B). Differences in digestion patterns obtained with Pb^{2+} ions and S1 nuclease could be explained by different sizes of these probes. S1 nuclease is a bulky enzyme (MW > 30 kDa), and some RNA regions accessible to Pb^{2+} ions might be protected from the enzyme, mainly stretches involved in the formation of a higher order RNA structure.

To further characterize the secondary structures of the selected Co^{2+}-binding aptamers and to search for potential interactions within their apical loops, chemical modification with DMS and CMCT was performed. The loop regions of both aptamers underwent extensive modification in the presence of both chemical reagents. Moreover, in aptamer no. 18, bases G25, A26, G27, G28, and A43 adjacent to the stem were protected from modification (Figure 4B). In the case of aptamer no. 20, neither bases G23, A24, G25, G26, and A45, which are located in the region adjacent to the helical stem, nor bases C36, G37, C38, G39, and G40 underwent modification.

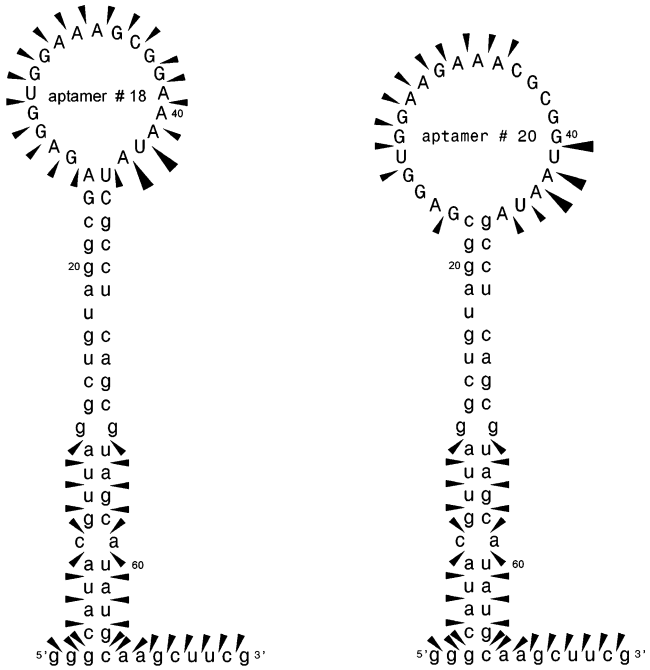

FIGURE 3: Results of Pb^{2+} probing of aptamer structures. Cleavages are displayed on stem−loop secondary structure models of aptamer no. 18 and no. 20. Lower and upper case letters indicate constant and randomized positions, respectively. Pb^{2+} cleavages are shown by black triangles. Intensity of cleavages is correlated with thickness of triangles.

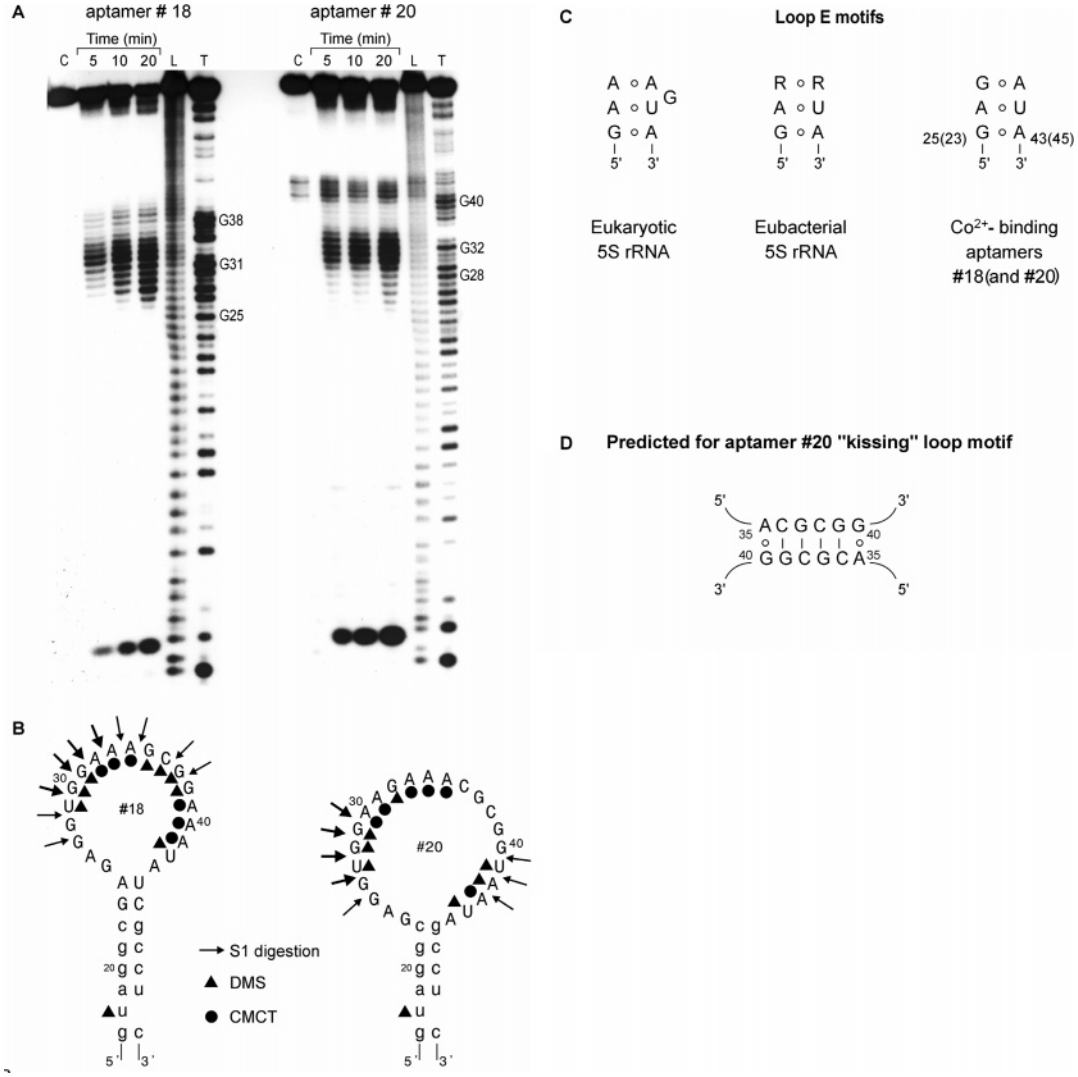

FIGURE 4: Structural probing of Co^2-binding aptamers with S1 nuclease as well as chemical reagents, DMS and CMCT. (A) Autoradiogram of S1 nuclease digestion experiment. Reactions were performed with 5′-end-labeled RNA at 25 °C for 10 min. Lanes are labeled as follows: C, reaction control; L, formamide ladder; T, limited hydrolysis by RNase T1. Guanine residues are labeled on the right. The enzyme at a 0.5 U/mL concentration was applied. (B) Summary of S1 nuclease and chemical modification probing data. The probing results of the loop regions of both aptamers are displayed. Lower and upper case letters indicate constant and randomized positions, respectively. (C) Structures of loop E-like motifs found in aptamer no. 18 and no. 20 and consensus structure of eukaryotic and eubacterial 5S rRNAs. (D) The "kissing" loop complex motif predicted for aptamer no. 20.

In general, the results of structural probing of aptamers no. 18 and no. 20 appear to be consistent with their loop/stem secondary structures. The experimentally established structures were also compared to those predicted by the mfold computer program (*29*). The structure of aptamer no. 18, as determined by biochemical probing (shown in Figure 3), and that predicted by the computer were identical. On the other hand, in aptamer no. 20, base-pairing between 26-GUG-28 and 36-CGC-38 stretches within the aptamer apical loop suggested by the mfold program was not supported by experimental data.

Closer examination of Pb^{2+} cleavage and S1 digestion, as well as chemical probing data, indicate possible involvement of some regions of the aptamers in the formation of noncanonical base pairs and/or participation in tertiary interactions. Stretches 25-GAGG-28 and 23-GAGG-26 in aptamers no. 18 and no. 20, respectively, are resistant to single-stranded specific probes. Possibly, these stretches are involved in the formation of E loop-like motifs. The motifs would extend the stem regions and consist of interactions G25−A43, A26−U42, and G27−A43 in the aptamer no. 18 or interactions G23−A45, A24−U44, and G25−A41 in the aptamer no. 20. (Figure 4C). Generally, a consensus model of loop E structure includes a sheared G−A pair followed by a reversed Hoogsteen A−U pair. The third noncanonical base pair is variable; however, in eubacterial 5S rRNA, two purines dominate in this position (*30*). Additionally, eukaryotic loop E motif contains a single bulged G residue (Figure 4C). Hence, the proposed E loop-like motifs occurring in Co^{2+}-binding aptamers are more related to the eubacterial consensus model (Figure 4C). Interestingly, in aptamer no. 20, also the sequence 36-ACGCGG-40 turns out to be resistant to single-stranded specific probes. We suggest that this partially self-complementary sequence might be responsible for the formation of a "kissing" loop complex structure, which is shown in Figure 4D. The dimer complex contains four canonical G−C or C−G Watson−Crick-type base pairs and a noncanonical sheared A−G interaction. As expected, only N1 of A35 is accessible to DMS modification, and G40 is not modified by CMCT.

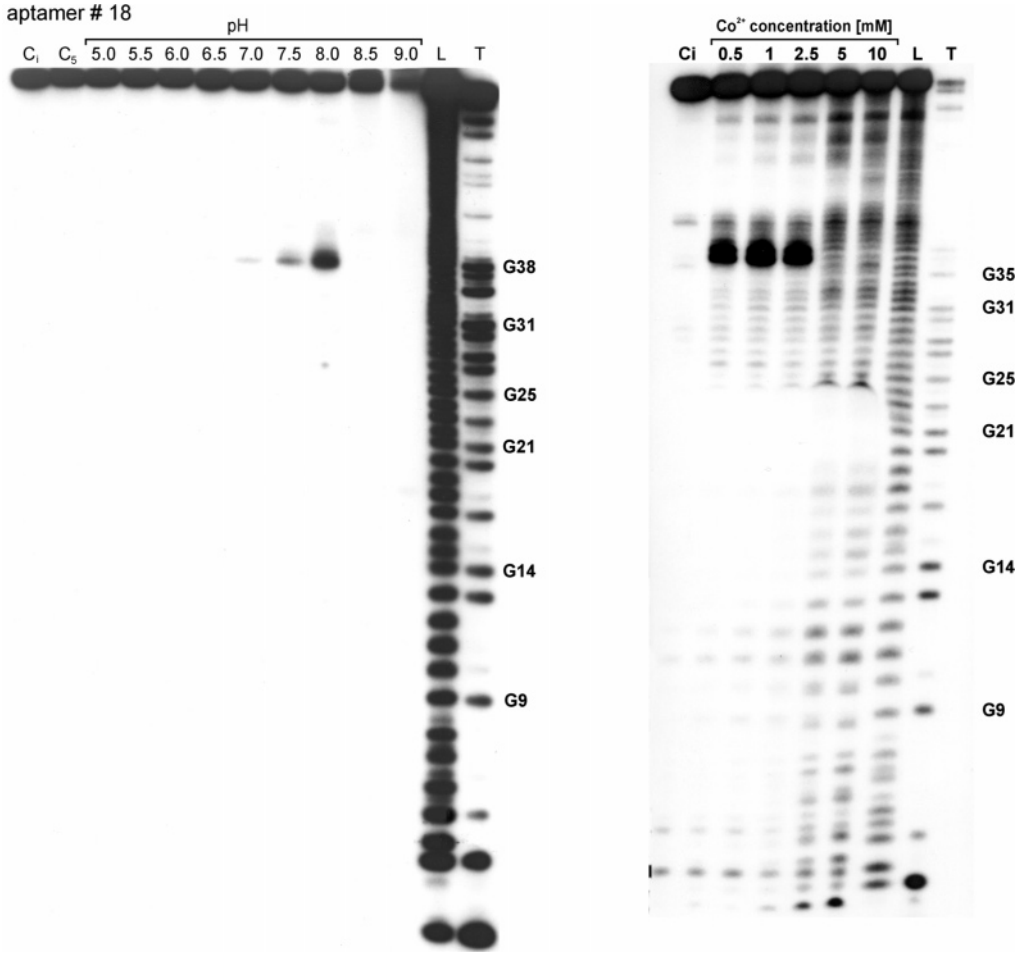

FIGURE 5: Dependence of Co^{2+}-induced cleavage reaction on pH (left panel) and metal ion concentration (right panel). Reaction was carried out with 5′-end-labeled RNA for 3 h at 37 °C in the following buffers: 50 mM sodium acetate (pH 5−6), 50 mM Hepes (pH 6.5−8.0), or 50 mM Tris-HCl (pH 8,5−9) in the presence of 40 mM NaCl and 2 mM Co^{2+} (pH dependence) or in 50 mM Hepes, pH 8.0 (concentration dependence). Lanes are labeled as follows: C_5, reaction control at pH 5.0; C_8, incubation control at pH 8.0; L, formamide ladder; T, limited hydrolysis by RNase T1. Guanine residues are labeled on the right.

We also examined the effect of 1 mM concentration of Co^{2+} on the aptamer structures by applying the same set of probes. Since there were no differences in the Pb^{2+} cleavage and chemical modification patterns, presumably, the structures of the loops are analogous in their Co^{2+} complexed and uncomplexed states (data not shown). This conclusion was mainly based on the results of chemical modification studies. There is a possibility, (suggested also by the manuscript reviewer), that the Pb^{2+} replaces bound Co^{2+} resulting in the same Pb^{2+}-induced cleavage patterns with and without Co^{2+}. In that case, Pb^{2+} cleavages might be less-diagnostic. More recently, using such methods as UV melting and DNA oligomer binding/RNase H digestion, we observed only a moderate increase in the stability of aptamers upon Co^{2+} binding without significant changes in their structures (manuscript in preparation). Generally, the lack of significant structural changes of aptamers after Co^{2+} binding indicates that they belong to the major class of RNAs which seem to contain preformed metal ion binding site (*6*).

Localization of Potential Co^{2+}-Binding Sites. Lack of information concerning conditions for Co^{2+}-induced RNA cleavage reaction prompted us to determine the optimal pH, Co^{2+} ion concentration, and reaction time. The pH dependence of Co^{2+}-induced cleavage of aptamer no. 18 showed that cleavages occurred only at pH values of 7.5 and 8.0 (Figure 5). This finding is rather unexpected since the pK_a value of Co^{2+} hydrate is 9.25 (Table 1), and according to the postulated reaction mechanism, we expected the maximum rate of cleavage to be at pH of 9.25, identical to the pK_a of Co^{2+} hydrate (*31*). The absence of Co^{2+}-induced cleavages at the pH 8.5 and 9.0 despite favorable ionization of the Co^{2+} aqua-cation is most likely due to the known tendency of precipitation of cobalt hydroxide, formation of polynuclear species at elevated pH (*32*). Another possibility, highlighted by the manuscript's reviewer, is switching of

Table 1: Physicochemical Properties of the Metal Ions Used in This Study[a]

divalent Me^{2+}	ionic radius (Å)	pK_a	coordination number	absolute hardness (η)
Mg^{2+}	0.72	11.4	6	47.59
Ca^{2+}	1.12	12.7	6, 8	19.52
Sr^{2+}	1.18	13.2	6	27.3
Ba^{2+}	1.35	13.8	6	
Zn^{2+}	0.74	9.6	6	10.88
Cd^{2+}	0.95	10.3	6	10.29
Ni^{2+}	0.69	9.7	4	8.50
$Co(NH_3)_6^{3+}$	0.61		6	8.9
Co^{2+}	0.75	9.25	6	8.22

[a] Data are taken from refs *5* and *63*.

purines coordination sites available for Co^{2+} ions at higher pH values (*33*). At lower, acidic pH, the N1 positions of inosine and guanosine are protonated and metal ions bind preferentially to N7 positions of bases. However, at higher pH, for example, over 8.5, predominant metal binding sites of purines are changed from N7 to N1 position after proton displacement. Thus, in Co^{2+}-induced RNA cleavage, the reaction pH should not exceed the value of 8. In Figure 5, the relationship between the efficiency of cleavage and concentration of Co^{2+} ions is shown. For aptamer no. 18, the rate of cleavage is similar within 0.5−2.5 mM Co^{2+} concentration range; however, at a concentration of 5 mM and higher, the reaction completely loses its specificity and cleavages at each phosphodiester bond are observed. It is most likely due to the depolymeryzation properties of Co^{2+} ions, which like some other metal ions, such as Pb^{2+}, Ni^{2+}, and Zn^{2+}, can degrade RNA molecules (*34*, *35*). Kinetic studies of Co^{2+}-induced cleavage of the selected aptamers showed doublet cleavages occurring at nucleotides G37, G38 and A31, G32, in aptamers no. 18 and no. 20, respectively (Figure 6). The cleavages were relatively weak, and the determined cleavage rate constants were 5.1×10^{-4} min^{-1} for aptamer no. 18 and 1.8×10^{-4} min^{-1} for aptamer no. 20. Since typical k_{obs} values determined for unspecific spontaneous cleavage of RNA is estimated to be 10^{-7} min^{-1} (*36*), Co^{2+}-induced cleavage is accelerated by at least 3 orders of magnitude. Additionally, we exploited the dependence of Co^{2+}-induced cleavage on the ion concentration to determine K_d values for binding of Co^{2+} to the selected aptamers. The K_d values determined by this approach were 0.50 ± 0.08 mM for aptamer no. 18 and 0.65 ± 0.11 mM for aptamer no. 20.

We extended our studies to Co^{2+}-induced RNA cleavage of yeast $tRNA^{Phe}$ molecule, in which several tightly bound Co^{2+} ions were precisely localized by X-ray crystallography (*37*). In Figure 7, kinetics of Co^{2+}-induced cleavage reaction of this tRNA is shown. Only a single cleavage site was observed at G15, and the calculated k_{obs}, ca. 8×10^{-4} min^{-1}, was comparable to that achieved with aptamer no. 18.

Effect of Various Metal Ions on Co^{2+}-Induced Cleavage. The Co^{2+}-induced cleavage of aptamers no. 18 and no. 20 occurring in the presence of various metal ions was applied to test metal ion specificity of the Co^{2+}-binding sites. It has been previously shown that the competition between a metal ion bound to RNA and another metal ion that can occupy the same binding site or is located in a close proximity usually affects the efficiency of metal ion-induced RNA cleavage (*38*). Seven metals with distinct chemical properties, namely, Mg^{2+}, Ca^{2+}, Sr^{2+}, and Ba^{2+} (group IIA in the periodic table) as well as Zn^{2+}, Cd^{2+}, and Ni^{2+} (transition metal ions) and, additionally, $Co(NH_3)_6^{3+}$ inert complex were tested as potential competitors (Table 1). The cleavage reactions were carried out at 2 mM concentration of Co^{2+} ions in the presence of 1 and 5 mM concentration of competitors, to replace Co^{2+} ions in their tight metal ion binding sites. The presence of Mg^{2+} had no influence on the extent of cleavage of aptamer no. 18, even after 3 h of incubation (Figure 8). Also, Ca^{2+} only slightly reduced the cleavage efficiency. For aptamer no. 18, an unexpected effect was observed in the presence of Sr^{2+} and Ba^{2+}. At a lower, 1 mM, concentration of these ions, cleavages were weakly inhibited. However, at a higher, 5 mM, concentration of Sr^{2+} and Ba^{2+}, the Co^{2+}-induced cleavage reaction was enhanced. In the presence of Ba^{2+}, the cleavage extent was increased by ca. 20%. An increase in the effective Co^{2+} concentration could be responsible for the observed phenomenon due to effective concentration increase of Co^{2+} in the cleavage site when nonspecifically bound Co^{2+} is being replaced by other metal ions as the manuscript reviewer pointed out. If this is the case, a similar effect might be observed at a higher concentration of monovalent ions. However, it turned out that at a higher NaCl concentration in the range of 10−100 mM such effect was not detected (data not shown). More-

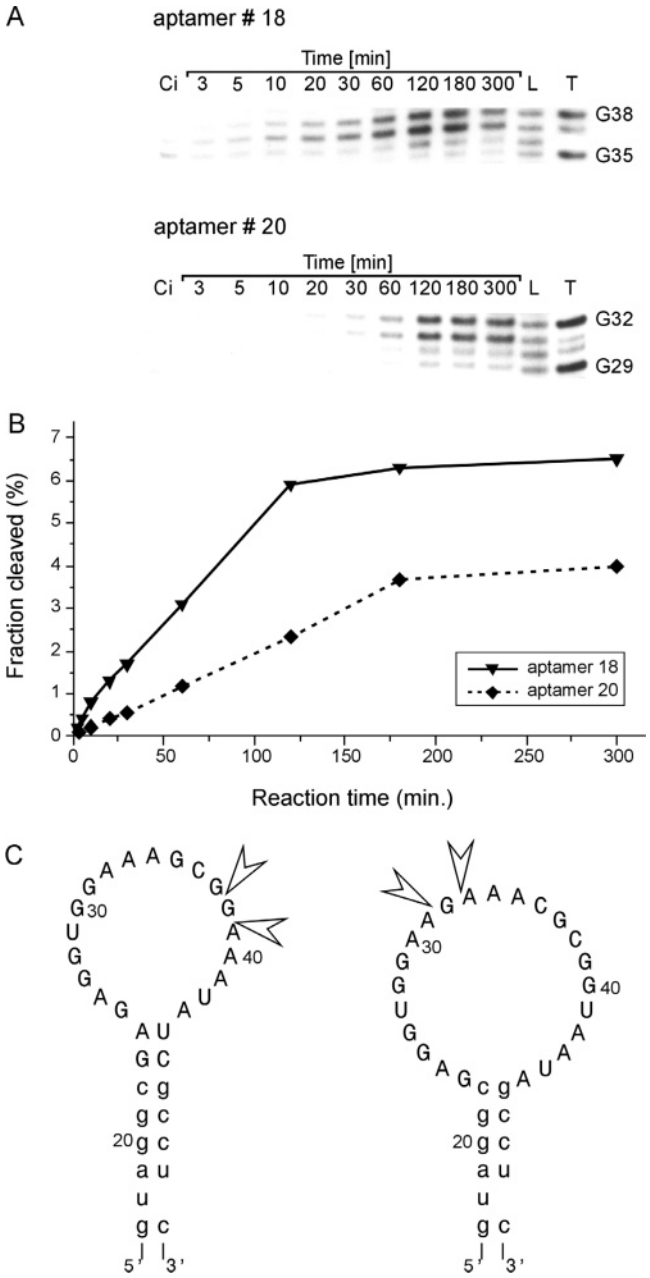

FIGURE 6: Kinetics of Co^{2+}-induced cleavages of aptamers no. 18 and no. 20. (A) Autoradiograms of cleavage reactions (only cleavage regions are shown). The reactions were carried out with 5′-end-labeled RNA in 50 mM Hepes, pH 8.0, 40 mM NaCl, and 2 mM Co^{2+}, at 37 °C. Lanes are labeled as follows: C, incubation control; L, formamide ladder; T, limited hydrolysis by RNase T1. Guanine residues are labeled on the right. (B) The cleavage efficiencies plotted as a function of time. (C) Locations of cleavage sites in the loop region of aptamers are shown (open arrows). Lower and upper case letters indicate constant and randomized positions, respectively.

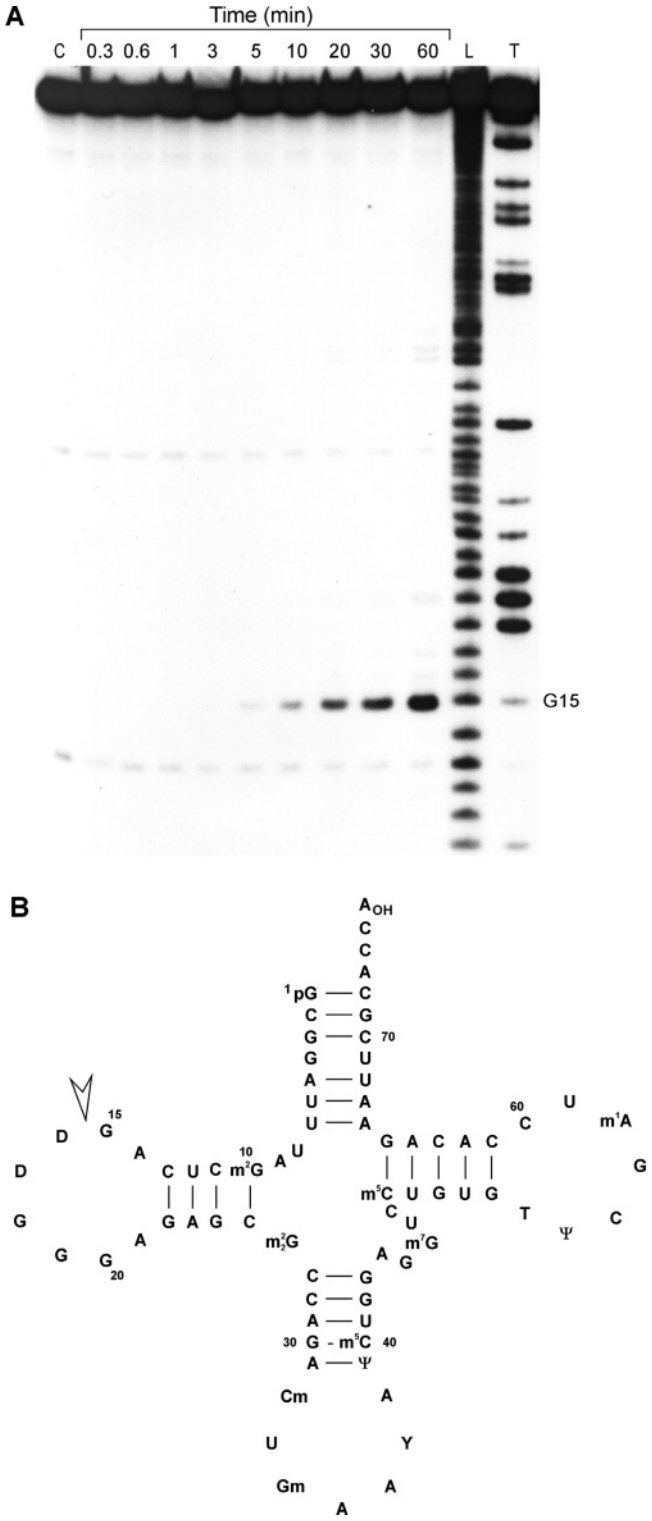

FIGURE 7: Kinetics of Co^{2+}-induced cleavage of yeast $tRNA^{Phe}$ (upper panel) and its cloverleaf structure with the major cleavage site marked by open arrow (lower panel). The reactions were carried out with 5′-end-labeled RNA in 50 mM Hepes, pH 8.0, 40 mM NaCl, and 2 mM Co^{2+}, at 37 °C. Lanes are labeled as follows: C, incubation control; L, formamide ladder; T, limited hydrolysis by RNase T1. Guanine residues are labeled on the right.

over, at a NaCl concentration higher than 200 mM, inhibition of cleavage efficiency was even observed. Thus, it seems that the suggested effect is not responsible for the observed cleavage enhancements. Interestingly, a similar synergetic effect, enhancement of Pb^{2+}-induced cleavage of leadzyme

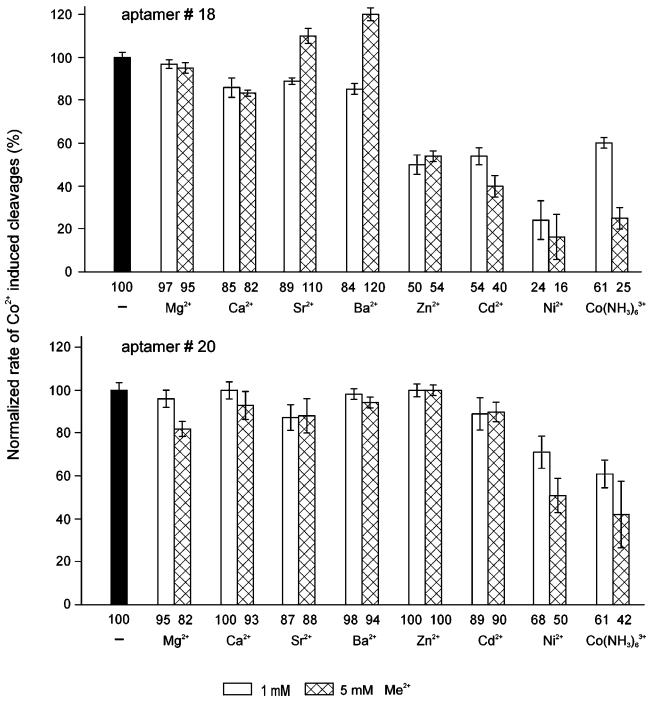

FIGURE 8: Inhibition of Co^{2+}-promoted cleavage of aptamers no. 18 and no. 20 by various divalent metal ions. The cleavage reactions were carried out with 5′-end-labeled RNA in 50 mM Hepes, pH 8.0, 40 mM NaCl, and 2 mM Co^{2+}, at 37 °C for 3 h in the presence of 1 or 5 mM concentration of selected divalent metal ions. The extent of cleavages was normalized and expressed as a percentage of uninhibited cleavage (black bar). Presented data are the mean of three independent experiments with standard deviations shown.

in the presence of Nd^{3+}, has been observed earlier (*39*). In contrast to alkaline metals, Zn^{2+} and Cd^{2+} significantly inhibited cleavages: at 5 mM concentration of these metals, the Co^{2+} cleavages were reduced by ca. 50%. In the case of aptamer no. 18, the highest inhibition occurred for Ni^{2+} and the $Co(NH_3)_6^{3+}$ complex (Figure 8). Even at low 1mM concentration of Ni^{2+}, as well as 5 mM concentration of the complex, the extent of Co^{2+}-induced cleavages reached no more than 25% of the values of uninhibited reactions. On the other hand, binding of Co^{2+} to aptamer no. 20 seemed to be more specific than to aptamer no. 18 (Figure 8). In the case of aptamer no. 20, the determined extents of Co^{2+}-induced cleavage in the presence of Mg^{2+}, Ca^{2+}, Sr^{2+}, and Ba^{2+} were comparable to the extents of uninhibited reactions. Moreover, the cleavage efficiencies were the same in the presence and absence of Zn^{2+} and Cd^{2+}, even at 5 mM concentration of these metals. On the other hand, in the case of aptamer no. 18, a very significant 50% inhibition of cleavage was observed. Strong inhibition occurred when Ni^{2+} and $Co(NH_3)_6^3$ were added to a Co^{2+}-promoted cleavage reaction of aptamer no. 20. However, the cleavage yields were at least twice as high as those achieved for aptamer no. 18.

DISCUSSION

In Vitro Selected Co^{2+}-Binding Aptamers. The K_d values, characterizing the binding of Co^{2+} to the in vitro selected aptamers, calculated by elution of RNA from metal ion affinity column, were significantly higher than the K_d values obtained using the Co^{2+}-induced cleavage method. The values determined by these two methods were 3.1 and 0.5

mM for aptamer no. 18 as well as 1.1 and 0.5 mM for aptamer no. 20. Divergencies in K_d values might be explained by different binding of free Co^{2+} ion and the ion bound to NTA-chelating groups. In solution, Co^{2+} ions form hexahydrates, and each H_2O molecule can be easily exchanged during RNA−metal interactions. The Co^{2+} ion bound to the NTA group contains only two exchangeable H_2O molecules in its coordination sphere, so possible interactions of that metal with RNA are limited. The determined K_d values indicate that the selected aptamers bind Co^{2+} with moderate affinity in the millimolar range. These values are typical of metal ion−RNA interactions. Most relative data concern binding of metal ions to ribozymes where K_d values were usually estimated as a concentration of metal required to reach a half of the maximum value of the k_{obs} constant. Such K_d values are in the range from 0.5 mM Mg^{2+} for *Tetrahymena* group I intron (*40*) to 36 mM Mg^{2+} for RNase P RNA (*41*). Hammerhead ribozyme exhibits an identical 3 mM K_d for three divalent metal ions, Mg^{2+}, Ca^{2+}, and Mn^{2+} (*15*). However, delta virus ribozyme shows different K_d values for active metal ions, 4.5 mM for Mg^{2+}, 3.5 mM for Ca^{2+}, and 2.5 mM for Mn^{2+} (*16*), similar to the K_d values of hairpin ribozyme, 3mM for Mg^{2+}, 10 mM for Sr^{2+}, and 20 mM for Ca^{2+} (*42*). Interestingly, the K_d of 1.1 mM for the aptamer that binds Zn^{2+} specifically, estimated by the isocratic elution method (*22*), is identical to the K_d determined by the same method for aptamer no. 20, which binds Co^{2+} ions. In contrast, the K_d for the Ni^{2+}-binding aptamer investigated by equilibrium dialysis is much lower, ca. 1 μM (*24*).

Both Co^{2+}-binding aptamers form the stem−loop secondary structures, which are consistent with the results of structural probing data. Very large apical loops consisting of 19 and 23 nucleotides for aptamers no. 18 and no. 20, respectively, suggest that these regions might be additionally structured. Thermodynamic studies of hairpins with homonucleotide loop sequences, in size ranging from three to nine nucleotides, have shown that the loops containing four or five nucleotides are the most stable (*43*). Furthermore, loops containing four nucleotides are prevalent in 16S rRNA (*44*), and some tetra loops, for example, UNCG and GNRA types show very high stability (*45*). Thus, the existence of other smaller RNA motifs within the loop region of aptamers could be expected. On the basis of our experimental results, we postulated formation of loop E-like and "kissing" loop complex motifs in the aptamer folds. The loop E motif has been found previously in 5S rRNA and 23S rRNA as well as in the hairpin ribozyme (*30*, *46*, *47*). The loop E-like motifs, present in the selected aptamers, are resistant to S1 nuclease digestion (Figure 4A,B), similarly to the loop E of *E. coli* 5S rRNA (*48*). Also, the chemical probing data are in line with the previously determined accessibility of loop E from *E. coli* 5S rRNA to chemical reagents (*46*).

In the first sheared A−G pair in the loop E structure determined by crystallography (*49*, *50*), only the N1 position of A is available to DMS modification. In the second reversed Hoogstein A−U pair, N6 of A forms a H-bond with O2 of U, and N7 of A interacts with N3 of U. Therefore, N1 of A is accessible to modification by DMS and N3 of U by CMCT, and indeed, only these positions are modified by these reagents in the loop E motifs of aptamer no. 18 and no. 20 as well as in *E. coli* 5S rRNA (*46*). In the third position of eubacterial loop E motif, a purine−purine base pair, usually A−A or G−G, occurs. However, in the selected aptamers, the G−A pair is present and only N1 of A is modified by DMS, similarly as in the first sheared G−A pair in the consensus loop E motif. Thus, we suggest that the first and third G−A pairs are structurally equivalent and possess a sheared G−A pair structure. Interestingly, an identical loop E-like structure has been found in Zn^{2+}-binding aptamer, and participation of this motif in the binding of divalent metal ions has been suggested (*22*).

It has been shown previously that dimerization of HIV virus is initiated at a stem/loop structure, at the so-called dimerization initiation site (DIS), and that the DIS motif is stabilized by formation of "kissing" loop interactions (*51*). The HIV-1 genome subtype B contains a six-nucleotide conservative sequence of the DIS 274-*GCGCGC*-279 (the self-complementary region is in italic type) (*52*). This sequence is similar to the 35-A*CGCG*G-40 stretch in aptamer no. 20, which might be involved in the formation of the "kissing" loop complex structure (Figure 4D). However, further studies are required to better characterize the "kissing" loop interactions proposed for aptamer no. 20.

Architecture of the Co^{2+}-Binding Site. We applied the Co^{2+}-induced cleavage method using optimal conditions determined in this work to detect a Co^{2+}-binding site in the selected aptamers as well as in yeast $tRNA^{Phe}$ molecule. This method has been widely used for the detection of the metal-binding site in several RNAs (*38*). In the presence of Co^{2+}, doublet cleavages at G37, G38 and A31, G32 were detected in aptamers no. 18 and no. 20, respectively, implying that these residues are involved in metal ion coordination.

In crystal structures of purine nucleotides GMP and IMP complexed with Co^{2+}, the metal ion is bound to the N7 position of nucleic bases. Usually, five water molecules are complexed to the metal, while the sixth water molecule of the octahedral coordination sphere is removed and the metal ion directly interacts with the N7 atom of the base (*53*). Some other RNA molecules, including the hammerhead ribozyme and yeast $tRNA^{Phe}$, bind Co^{2+} in a similar manner. The crystal structure of the hammerhead ribozyme contains Co^{2+} that is located approximately 2.5 Å from N7 of G5 and shares the outer sphere coordination (*54*). Additionally, binding of this ion induces a conformational change and creates a site for another Co^{2+} located 2.3 Å from N7 of A1.1 with the inner sphere coordination and near the 5′ oxygen of the leaving group. A recently resolved crystal structure of the monoclinic form of yeast $tRNA^{Phe}$ has allowed to precisely determine five Co^{2+}-binding sites (*37*). In most of them, Co^{2+} ions bind to the N7 position of guanine residues. Co^{2+} bound to N7 of G15 is of particular interest as this ion has previously been detected in the crystal structure of $tRNA^{Phe}$ resolved with a lower resolution and its direct interaction with N7 of G15 with 2,2 Å distance has been postulated (*55*). Coordination of Co^{2+} to the G15 residue presumably occurs also in solution, because in the NMR spectra of tRNA, the U8−A14 resonance in proximity to G15 is paramagnetically relaxed after addition of Co^{2+} (*56*).

Our experimental data on Co^{2+}-induced cleavage of yeast $tRNA^{Phe}$ revealed a single cleavage site at G15. This clearly suggests that the Co^{2+} ion coordinated to the N7 atom of G15 might be responsible for strand breakage. Taking into account a very high affinity of N7 imino atoms of purines toward Co^{2+} ions in the aforementioned RNAs and the ability

of such coordinate metal ion to promote specific cleavage of RNA chain, we propose a similar organization of metal ion binding site in the selected Co^{2+}-binding aptamers. In this model, a Co^{2+} ion directly bound to N7 atom of adenine or guanine residues, in its strong binding site, interacts with a neighboring 2′OH group and promotes cleavage of phosphodiester linkage. A possibility that the metal ion is coordinated somewhere else in the aptamer structures, for example, to the loop E or "kissing" loop complex motifs, and that this ion promotes cleavage of phosphodiester linkage remote in the secondary structure but close spatially cannot be definitely excluded; however, it seems rather unlikely.

Metal Ion Specificity of Co^{2+}-Binding Motifs. We tested the influence of seven chemically distinct metal ions as well as chemically inert cobalt(III)hexamine complex on Co^{2+}-promoted cleavage of the selected aptamers. Two groups of metals were distinguished. Alkaline metal ions Mg^{2+}, Ca^{2+}, Sr^{2+}, and Ba^{2+} did not affect Co^{2+}-induced cleavages. However, transition metal ions Ni^{2+} and $Co(NH_3)_6^{3+}$ significantly inhibited the reaction in aptamer no. 20. In aptamer no. 18, a broader spectrum of metals, Ni^{2+}, $Co(NH_3)_6^{3+}$, Zn^{2+}, and Cd^{2+}, affected the cleavage reaction. It seems that transition metal ions display affinity to the Co^{2+}-binding pocket, displacing strongly bound Co^{2+} and influencing the RNA cleavage. Binding preferences of alkaline metals and Co^{2+} to RNA are quite different; thus, these ions do not replace Co^{2+} ions in their strong metal-binding sites. The comparison of the physical and chemical properties of metals which were used in our studies (Table 1) indicates that either their ionic radius or coordination number are not decisive in the discrimination of alkaline and transition metals by the Co^{2+}-binding pockets. However, binding properties are well described in terms of metal ion absolute hardness (η). Metals with high values of η ("hard metals") bind preferentially to nonbridging oxygen atoms of phosphate groups, while transition metals ("soft metals") with low η values show affinity to N and S atoms of bases (*5*). Thus, in the selected aptamers, coordination of Co^{2+} to the N7 positions of purines prevails over binding to phosphate groups. Divergent affinity of Zn^{2+} and Cd^{2+} to aptamers no. 18 and no. 20 might reflect their different secondary/tertiary structures; in particular, the "kissing" loop complex motif seems to be present only in aptamer no. 20.

Multiple metal ion specificity has been observed previously for several RNA molecules. The application of the Pb^{2+} cleavage method to Zn^{2+}-binding aptamer has allowed to identify metal ions that interfered with the extent of Pb^{2+}-induced RNA cleavage. In addition to Zn^{2+}, Co^{2+}, Ni^{2+}, and Cd^{2+} have also inhibited the reaction (*22*). The Ni^{2+}-binding aptamer has showed a similarly high affinity ($K_d \sim 1$ μM) to Ni^{2+} as to Co^{2+} (*24*). The formation of a stable RNA aptamer−biocytin complex mediated by Ni^{2+} has been moderately inhibited in the presence of Co^{2+} as well as Mn^{2+} and Mg^{2+} (*57*). Recently, Breaker and co-workers have constructed an allosteric ribozyme containing a Co^{2+}-sensing module (*58*). They have observed a significant enhancement of cleavage, even at a low concentration of Co^{2+} ($K_d \sim 500$ μM). However, the same activity of ribozyme has been triggered by Ni^{2+}, Zn^{2+}, and Cd^{2+}. Interestingly, in this work, we observed a similar metal ion specificity for aptamer no. 18. In some naturally occurring RNAs, replacement of Co^{2+} by other metal ions has also been described. For example, in yeast $tRNA^{Phe}$, in which the exact location of several metal ions has been determined, Co^{2+} in its binding pocket, might be replaced by Mn^{2+} (*37*). However, in the next two binding sites, primarily identified to be Mg^{2+} sites, Co^{2+} displaces this metal ion. Replacement of Mg^{2+} by Mn^{2+}, Zn^{2+}, and Co^{2+} has also been observed in the subtype-A DIS structure (*59*). These three metals share similar binding properties and bind to the same site found for Mg^{2+}, that is, in the major groove to N7 and O6 atoms of guanine residues.

In both aptamer no. 18 and no. 20, we observed a significant inhibition of Co^{2+}-induced cleavages in the presence of Co(III)hexammine. This complex has frequently been used in biochemistry, NMR spectroscopy, and crystallography, since it perfectly mimics the physiologically important hydrated magnesium ion due to similar ionic radius and octahedral hydratation geometry (*60*−*62*). Moreover, inhibition of Co^{2+}-induced cleavage indicates that this complex is able to replace not only Mg^{2+} but also Co^{2+} ions in their strong binding sites.

Finally, a comparison of metal specificity of in vitro selected Co^{2+}-binding aptamers with the metal specificity of other aptamers and naturally occurring RNAs shows that most of the Co^{2+}-binding motifs are multi-ion specific and that tightly bound Co^{2+} can be replaced by some other transition metal ions. A similar specificity of motifs derived from aptamers and natural RNAs suggests that these molecules use essentially the same principles for creating metal ion binding sites. Thus, the application of the in vitro selection methodology in the search for other motifs, also with other metal ion specificities, should further help to better understand the determinants that contribute to metal ion−RNA interactions and also those found in the nature.

ACKNOWLEDGMENT

We thank Michal Brzustowski for his contribution at the early stage of the project and Barbara Smolska for her excellent technical assistance. We also thank the reviewers for comments on the manuscript.

REFERENCES

1. Frausto da Silva, J. J., and Williams, R. J. (2000) Molybdenum, tungsten, vanadium and chromium, in *The Biological Chemistry of the Elements. The Inorganic Chemistry of Life*, pp 450−470, Oxford University Press, Oxford, U.K.
2. Volbeda, A., Fontecilla-Camps, J., and Frey, M. (1996) Novel metal sites in protein structures, *Curr. Opin. Struct. Biol. 6*, 804−812.
3. Swiatek, J. (1994) Interactions of metal ions with nucleic acids and their subunits, *J. Coord. Chem. 33*, 191−217.
4. Pan, T., Long, D. M., and Uhlenbeck, O. C. (1993) Divalent metal ions in RNA folding and catalysis, in *RNA World* (Gesteland, R. F., and Atkins, J. F., Eds.) pp 271−302, Cold Spring Laboratory Press, Plainview, NY.
5. Feig, A. L., and Uhlenbeck, O. C. (1999) The role of metal ions in RNA biochemistry, in *RNA World* (Gesteland, R. F., Cech, T. R., and Atkins, G., Eds.) pp 287−319, Cold Spring Laboratory Press, Plainview, NY.
6. Tinoco, I., Jr., and Bustamante, C. (1999) How RNA folds, *J. Mol. Biol. 293*, 271−281.
7. Hermann, T., and Patel, D. J. (1999) Stitching together RNA tertiary architectures, *J. Mol. Biol. 294*, 829−849.
8. Narlikar, G. J., and Herschlag, D. (1997) Mechanistic aspects of enzymatic catalysis: lessons from comparison of RNA and protein enzymes, *Annu. Rev. Biochem. 66*, 19−59.
9. Pyle, A. (2002) Metal ions in the structure and function of RNA, *J. Biol. Inorg. Chem. 7*, 679−690.

10. Kruger, K., Grabowski, P. J., Zaug, A. J., Sands, J., Gottschling, D. E., and Cech T. R. (1982) Self-splicing RNA: autoexcision and autocyclization of the ribosomal RNA intervening sequence of Tetrahymena, *Cell 31*, 147−157.
11. Guerrier-Takada, C., Gardiner, K., Marsh, T., Pace, N., and Altman, S. (1983) The RNA moiety of ribonuclease P is the catalytic subunit of the enzyme, *Cell 35*, 849−857.
12. Doudna, J. A., and Cech, T. R. (2002) The chemical repertoire of natural ribozymes, *Nature 418*, 222−228.
13. Misra, V. K., and Draper, D. E. (1998) On the role of magnesium ions in RNA stability, *Biopolymers 48*, 113−135.
14. Kobayashi, M., and Shimuzu, S. (1999) Cobalt proteins, *Eur. J. Biochem.* 261, 1−9.
15. Dahm, S. C., and Uhlenbeck, O. C. (1991) Role of divalent metal ions in the hammerhead RNA cleavage reaction, *Biochemistry 30*, 9464−9469.
16. Wrzesinski, J., Legiewicz, M., Smolska, B., and Ciesiolka, J. (2001) Catalytic cleavage of cis- and trans-acting antigenomic delta ribozymes in the presence of various divalent metal ions, *Nucleic Acids Res. 29*, 4482−4492.
17. Winkler, W. C., Nahvi, A., Roth, A., Collins, J. A., and Breaker, R. R. (2004) Control of gene expression by a natural metabolite-responsive ribozyme, *Nature 428*, 281−286.
18. Famulok, M. (1999) Oligonucleotide aptamers that recognize small molecules, *Curr. Opin. Struct. Biol. 9*, 324−329.
19. Wilson, D. S., and Szostak, J. W. (1999) In vitro selection of functional nucleic acids, *Annu. Rev. Biochem. 68*, 611−647.
20. Matysiak, M., Wrzesinski, J., and Ciesiolka, J. (1999) Sequential folding of the genomic ribozyme of the hepatitis delta virus: structural analysis of RNA transcription intermediates, *J. Mol. Biol. 291*, 283−294.
21. Milligan, J. F., and Uhlenbeck, O. C. (1989) Synthesis of small RNAs using T7 RNA polymerase, *Methods Enzymol. 180*, 51−62.
22. Ciesiołka, J., Gorski, J., and Yarus, M. (1995) Selection of an RNA domain that binds Zn^{2+}, *RNA 1*, 538−550.
23. Ciesiołka, J., and Yarus, M. (1996) Small RNA-divalent domains, *RNA 2*, 785−793.
24. Hofmann, H. P., Limmer, S., Hornung, V., and Sprinzl, M. (1997) Ni^{2+}-binding RNA motifs with an asymmetric purine-rich internal loop and a G−A base pair, *RNA 3*, 1289−1300.
25. Giege, R., Helm, M., and Florentz, C. (1999) Chemical and enzymatic probing of RNA structure, in *Comprehensive Natural Product Chemistry* (Soll, D., and Nishimura, S., Eds.) pp 63−80, Pergamon Press, Oxford, U.K.
26. Markley, J. C., Godde, F., and Sigurdsson, S. Th. (2001) Identification and characterization of a divalent metal ion-dependent cleavage site in the hammerhead ribozyme, *Biochemistry 40*, 13849−13856.
27. Ciesiolka, J., Illangasekare, M., Majerfeld, I., Nickles, T., Welch, M., Yarus, M., and Zinnen, S. (1996) Affinity selection-amplification from randomized ribooligonucleotide pools, *Methods Enzymol. 267*, 315−335.
28. Ciesiolka, J., Michalowski, D., Wrzesinski, J., Krajewski, J., and Krzyzosiak, W. J. (1998) Patterns of cleavages induced by lead ions in defined RNA secondary structure motifs, *J. Mol. Biol. 275*, 211−220.
29. Zuker, M., Mathews, D. H., and Turner, D. H. (1999) Algorithms and thermodynamics for RNA secondary structure prediction: a practical guide, in *RNA Biochemistry and Biotechnology* (Barciszewski, J., and Clark, B. F. C., Eds.) pp 11−43, NATO ASI Series, Kluwer Academic Publishers, Dordrecht, The Nederlands.
30. Szymanski, M., Barciszewska, M. Z., Erdmann, V. A., and Barciszewski, J. (2002) 5S Ribosomal RNA database, *Nucleic Acids Res. 30*, 176−178.
31. Brown, R. S., Hingerty, B. E., Dewan, J. C., and Klug, A. (1983) Pb(II)-catalysed cleavage of the sugar−phosphate backbone of yeast tRNAPhe−implications for lead toxicity and self-splicing RNA, *Nature 303*, 543−546.
32. Burgess, J. (1978) Polymerisation, in *Metal Ion in Solution*, pp 290−309, Harwood, Chichester, UK.
33. Lonnberg, H., and Vihanto, P. (1981) Complexing of inosine and guanosine with divalent metal ions in aqueous solution, *Inorg. Chim. Acta 56*, 157−161.
34. Butzow, J. J., and Eichhorn, G. L. (1965) Interactions of metal ions with polynucleotides and related compounds, *Biopolymers 3*, 95−107.
35. Farkas, W. R. (1968) Depolymerization of ribonucleic acid by plumbous ion, *Biochim. Biophys. Acta 155*, 401−409.
36. Li, Y., and Breaker, R. R. (1999) Kinetics of RNA degradation by specific base catalysis of transesterification involving the 2′ hydroxyl group, *J. Am. Chem. Soc. 121*, 5364−5572.
37. Shi, H., and Moore, P. B. (2000) The crystal structure of yeast phenylalanine tRNA at 1.93 Å resolution: a classic structure revisited, *RNA 6*, 1091−1105.
38. Kirsebom, L A., and Ciesiolka, J. (2005) Pb^{2+}-induced cleavage of RNA, in *Handbook of RNA Biochemistry*, (Hartmann, R. K., Bindereif, A., Schon, A., Westhof, E. Eds.) pp 214−228, Wiley-VCH GmbH & Co, KGaA, Weinheim, Germany.
39. Ohmichi, T., and Sugimoto, N. (1997) Role of Nd^{3+} and Pb^{2+} on the RNA cleavage reaction by a small ribozyme, *Biochemistry 36*, 3514−3521.
40. Grosshans, C. A., and Cech, T. R. (1989) Metal ion requirements for sequence-specific endoribonuclease activity of the *Tetrahymena* ribozyme, *Biochemistry 28*, 6888−6894.
41. Beebe, J. A., Kurz, J. C., and Fierke, C. A. (1996) Magnesium ions are required by *Bacillus subtilis* ribonuclease P RNA for both binding and cleaving precursor $tRNA^{Asp}$, *Biochemistry 35*, 10493−10505.
42. Chowrira, B. M., Berzal-Herranz, A., and Burke, J. M. (1993) Ionic requirements for RNA binding, cleavage, and ligation by the hairpin ribozyme, *Biochemistry 32*, 1088−1095.
43. Groebe, D. R., and Uhlenbeck, O. C. (1988) Characterization of RNA hairpin loop stability, *Nucleic Acids Res. 16*, 11725−11735.
44. Woese, C. R., Winker, S., and Gutell, R. R. (1990) Architecture of ribosomal RNA: constraints on the sequence of "tetra-loops", *Proc. Natl. Acad. Sci. U.S.A. 87*, 8467−8471.
45. Antao, V. P., Lai, S. Y., and Tinoco, I., Jr. (1991) A thermodynamic study of unusually stable RNA and DNA hairpins, *Nucleic Acids Res. 19*, 5901−5905.
46. Leontis, N. B., and Westhof, E. (1998) The 5S rRNA loop E: chemical probing and phylogenetic data versus crystal structure, *RNA 4*, 1134−1153.
47. Butcher, S., Allain, F. H.-T., and Feigon, J. (1999) Solution structure of the loop B domain from the hairpin ribozyme, *Nat. Struct. Biol. 6*, 212−216.
48. Brunel, C., Romby, P., Westhof, E., Ehresmann, C., and Ehresmann, B. (1991) Three-dimensional model of *Escherichia coli* ribosomal 5 S RNA as deduced from structure probing in solution and computer modeling, *J. Mol. Biol. 221*, 293−308.
49. Corell, C. C., Freeborn, B., Moore, P. B., and Steitz, T. A. (1997) Metals, motifs, and recognition in the crystal structure of a 5S rRNA domain, *Cell 91*, 705−712.
50. Lu, M., and Steitz, T. A. (2000) Structure of *Escherichia coli* ribosomal protein L25 complexed with a 5s rRNA fragment at 1.8-Å resolution, *Proc. Natl. Acad. Sci. U.S.A. 97*, 2023−2028.
51. Paillart, J. C., Marquet, R., Skripkin, E., Ehresmann, C., and Ehresmann, B. (1996) Dimerization of retroviral genomic RNAs: structural and functional implications, *Biochimie 78*, 639−653.
52. Paillart, J. C., Marquet, R., Skripkin, E., Ehresmann, B., and Ehresmann, C. (1994) Mutational analysis of the bipartite dimer linkage structure of human immunodeficiency virus type 1 genomic RNA, *J. Biol. Chem. 269*, 27486−27493.
53. Sigel, H., and Song, B. (1996) Solution structures of nucleotide−metal ion complexes. Isomeric equilibria, in *Metals Ions in Biological Systems* (Sigel, H., and Sigel, A., Eds) pp 135−205, Markel Decker Inc., New York and Basel.
54. Marray, J. B., Terwey, D. P., Maloney, L., Karpeiski, A., Usman, N., Baigelman, L., and Scott, W. G. (1998) The structure basis of hammerhead ribozyme self-cleavage, *Cell 92*, 665−673.
55. Jack, A., Ladner, J. E., Rhodes, D., Brown, R. S., and Klug, A. (1977) A crystallographic study of metal-binding to yeast phenylalanine transfer RNA, *J. Mol. Biol. 111*, 315−328.
56. Hurd, R. E., Azhderian, E., and Reid, B. R. (1979) Paramagnetic ion effects on the nuclear magnetic resonance spectrum transfer ribonucleic acid: assignment of the 15−48 tertiary resonance, *Biochemistry 18*, 4012−4017.
57. Hati, S., Boles, A. R., Zaborske, B. B., Posto, A. L., and Burke, D. H. (2003) $Nickel^{2+}$-mediated assembly of an RNA−amino acid complex, *Chem. Biol. 10*, 1129−1137.
58. Seetharaman, S., Zivarts, M., Sudarsan, N., and Breaker, R. R. (2001) Immobilized RNA switches for the analysis of complex chemical and biological mixtures, *Nat. Biotechnol. 19*, 336−341.
59. Ennifar, E., Walter, P., and Dumas, P. (2003) A crystallographic study of the binding of 13 metal ions to two related RNA duplexes, *Nucleic Acids Res. 31*, 2671−2682.

60. Kieft, J. S., and Tinoco, I. J. (1997) Solution structure of a metal-binding site in the major groove of RNA complexed with cobalt (III) hexammine, *Structure 5*, 713−721.
61. Rudisser, S., and Tinoco, I. T., Jr. (2000) Solution structure of Cobalt (III)hexammine complexed to the GAAA tetraloop, and metal-ion binding to G A mismatches, *J. Mol. Biol. 295*, 1211−1223.
62. Gonzales, R. L., and Tinoco, I. J. (2000) Identification and characterization of metal ion binding sites in RNA, *Metods Enzymol. 338*, 443−521.
63. Burgess, J. (1978) Hydrolysis, in *Metal Ion in Solution*, pp 259−289, Harwood, Chichester, UK.

BI047397U